OPEN ACCESS

International
Journal
Of Modern Engineering Research (IJMER)

Comparison of Different Absorbing Boundary Conditions for GPR Simulation by the Time Domain Finite Element Method

ZhiyongZhang[1,2], Man Li[1]
1,(School of Geosciences and Info-Physics, Central South University)
2, (School of Nuclear Engineering and Geophysics, East China Institute of Technology)

Abstract:*This paper compares three boundary conditions, i.e. transmitting boundary condition, Sarma absorbing boundary condition and the uniaxial complete matched layerabsorbing boundary condition for simulation of ground penetrating radar (GPR) by the time domain finite element (FEM) method. The formulations of the three boundary conditions for the FEM method are described. Their effectiveness in absorbing the incident electromagnetic waves are evaluated by the reflection coefficient on the boundary of a simple GPR model.The results demonstrate that UPML boundary condition can yield a reflection coefficient smaller than -50 dB, which is -20 dB smaller than other two boundary conditions.*

Keywords:*Ground penetrating radar (GPR);uniaxial complete matched layer absorbing boundary condition; Sarma boundary condition, transmitting boundary condition; finite element method*

I. Introduction

Ground penetrating radar (GPR) has been widely applied in many fields. Numerical simulation plays a great role in the interpretation of GPR data and the inversion of physical parameters. Finite element method (FEM) is widely used due to its easy adaption to a complex subsurface dielectric model with a triangle mesh. Shen et al [9]have performed a 2D forward GPR modeling by substituting the electromagnetic wave transmitting equation with the sound wave equation; Di and Wang [10] introduces the complex dielectric permittivity into the finite element equation using the Galerkin method. Tiao et al [11]perform a GPR numerical simulation on dispersive media using a discrete time-domain method. Arias et al [12] applies the GPR finite element technique to the imaging of archaeological remains. For GPR numerical simulation, absorbing boundary condition is indispensable for eliminating the undesired boundary reflection. An effective absorbing boundary condition is critical for improvement of the accuracy of GPR numerical simulation. Many research efforts have been paid to the absorbing boundary conditions for the GPR forward modelling using the finite different time domain (FDTD) algorithm. There are several absorbing boundary conditions working with different Attenuation mechanisms. For an example, the radiant boundary condition (Bayliss and Turkel E. 2009) and absorbing boundary condition are based on the separate wave equation(Engquist and Majda. 1977); ultra-absorbing boundary condition (Mei. 1992), and complete matched layer(Gedney et al. 2001; Berenger. 1994,) absorbing boundary condition have been applied. For the GPR simulation by the FEM method, Di and Wang (2005) use a transmitting absorbing boundary condition; Sarma absorbing condition has been used in GPR 2D numerical simulation by Feng (2013). UPML absorbing boundary condition also has applied in GPR 2D dispersive medium numerical simulation (Tiao L, 2006). In this paper, the principle and the formulations of the transmission absorbing, Sarma absorbing and UPML absorbing boundary conditions are going to be presented. Their performances while applied to the FEM simulation are tested.

II. Fem Applied To Wave Equation Of Gap

The electric field radiated by a GPR source is governed by wave equation, as expressed by (Di, et al., 1999)

$$\frac{\partial^2 \boldsymbol{E}}{\partial t^2} - \frac{\nabla^2 \boldsymbol{E}}{\mu\varepsilon} + \frac{\sigma}{\varepsilon}\partial \boldsymbol{E} / \partial t = \boldsymbol{S}_E \qquad (1)$$

where ε is the dielectric permittivity, μ is the magnetic permeability, σ is the electrical conductivity, $\boldsymbol{E}$ is electric-field intensity and $\boldsymbol{S}_E$ is the electric field source. We divide the 2D region into rectangular elements and let $\boldsymbol{E}$ be a linear function of position coordinates in each element, as given by

$$\boldsymbol{E} = \boldsymbol{N}^T \boldsymbol{E}_e \quad (2)$$

where $\boldsymbol{N}$ is the shape function for linear interpolation and $\boldsymbol{E}_e$ is the column vector whose components are $\boldsymbol{E}_i$ at the node i of the element where $i = 1, 2, 3, 4$. Using the Galerkin method, the general 2D finite-element

equation in time and spatial domain can be expressed as

$$\boldsymbol{M}\ddot{\boldsymbol{E}} + \boldsymbol{K}'\dot{\boldsymbol{E}} + \boldsymbol{K}\boldsymbol{E} = \boldsymbol{S}_E \quad (3)$$

where $\boldsymbol{M}$ is the mass matrix, $\boldsymbol{K}'$ is the damping matrix, $\boldsymbol{K}$ is the stiffness matrix, $\dot{\boldsymbol{E}}$ and $\ddot{\boldsymbol{E}}$ are the first- and second-order derivatives of electric field, respectively.We can adopt the central difference method in time domain to solve the Eq. (3).

III. Absorbing Boundary Conditions

In this section, we apply the transmitting boundary condition, sarmaboundary condition and UPML absorbing boundary condition to the FEM simulation of GPR data.

3.1 Transmitting boundary condition

The transmitting boundary condition is established by directly simulating the common kinematic properties of various one-way waves. The principle is that the one-way waves are transmitted through the boundary interface at one point on the artificial boundary. This means that the one-way waves can be expressed as the superposition of a series of outgoing plane waves, because there is no specific limit to the speed at which these plane waves transmit along the artificial boundary, nor any limitation on their shapes. Assuming that all the one-way waves are transmitted along artificialboundary at the same velocity, we obtain a formula for the transmitting boundary condition[24-25].

Suppose

$$L\boldsymbol{E} = \frac{\partial^2 \boldsymbol{E}}{\partial t^2} - \frac{1}{\mu\varepsilon}\nabla^2 \boldsymbol{E} + \frac{\sigma}{\varepsilon}\frac{\partial \boldsymbol{E}}{\partial t} = \boldsymbol{S}_E . \quad (4)$$

At each element, the electrical field $\boldsymbol{E}$ can be expressed as

$$\boldsymbol{E} = \sum_{i=1}^{4} N_i E_i , \quad (5)$$

where E_i and N_i refer to the electric field and the shape function of the node i in each element. The residual quantity $\boldsymbol{R}$ can be expressed as

$$\boldsymbol{R} = L\boldsymbol{E} - \boldsymbol{S}_E . \quad (6)$$

According to the Galerkinfinite element method, the 2D finite element equation can be expressed as

$$\sum_e \int_\Omega \boldsymbol{N}^T \boldsymbol{r} dxdy = 0 , \quad (7)$$

where Ω refers to the area of the element and $\boldsymbol{r}$ is the vector expression of $\boldsymbol{R}$ .According to the paraxial approximation deduced by Clear.bout[26], the down-going, up-going, left-going, right-going wave equations in a homogeneous isotropic medium, arerespectively expressed as

$$\frac{\partial \boldsymbol{E}}{\partial t} = \frac{1}{v}\frac{\partial \boldsymbol{E}}{\partial y}, \frac{\partial \boldsymbol{E}}{\partial t} = -\frac{1}{v}\frac{\partial \boldsymbol{E}}{\partial y}, \frac{\partial \boldsymbol{E}}{\partial t} = -\frac{1}{v}\frac{\partial \boldsymbol{E}}{\partial x}, \frac{\partial \boldsymbol{E}}{\partial t} = \frac{1}{v}\frac{\partial \boldsymbol{E}}{\partial x}, \quad (8)$$

According to the definition of the normal derivative, we know that

$$\frac{\partial}{\partial n} = \frac{\partial}{\partial x} n_x + \frac{\partial}{\partial y} n_y , \quad (9)$$

where n_x and n_y refer to the direction cosines of the boundary external normal.By importing Eq. (5) and (6) into Eq. (7) and applying Gauss theory, we can obtained

$$\sum_e \int_\Omega \frac{\partial}{\partial x}\left(\frac{\partial \boldsymbol{E}^T}{\partial x}\boldsymbol{N}\right) dxdy = \int_{\Gamma_l} \frac{\partial \boldsymbol{E}^T}{\partial n}\boldsymbol{N} d\Gamma + \int_{\Gamma_d} \frac{\partial \boldsymbol{E}^T}{\partial n}\boldsymbol{N} d\Gamma + \int_{\Gamma_r} \frac{\partial \boldsymbol{E}^T}{\partial n}\boldsymbol{N} d\Gamma \int_{\Gamma_u} \frac{\partial \boldsymbol{E}^T}{\partial n}\boldsymbol{N} d\Gamma , \quad (10)$$

where $\Gamma_l, \Gamma_r, \Gamma_d, \Gamma_u$ representthe left, right, bottom, upper boundary respectively. Importing the boundary conditions of Eq. (9) into Eq. (10) we can obtained

$$\int_{\Gamma_l}\frac{\partial \boldsymbol{E}^T}{\partial n}\boldsymbol{N}d\Gamma+\int_{\Gamma_d}\frac{\partial \boldsymbol{E}^T}{\partial n}\boldsymbol{N}d\Gamma+\int_{\Gamma_r}\frac{\partial \boldsymbol{E}^T}{\partial n}\boldsymbol{N}d\Gamma+\int_{\Gamma_u}\frac{\partial \boldsymbol{E}^T}{\partial n}\boldsymbol{N}d\Gamma$$
$$=v\dot{\boldsymbol{E}}\times\begin{pmatrix}\int_{\Gamma_l}N_1N_2\left(n_x+n_y\right)d\Gamma+\int_{\Gamma_d}N_2N_3\left(n_x+n_y\right)d\Gamma\\+\int_{\Gamma_r}N_3N_4\left(n_x+n_y\right)d\Gamma+\int_{\Gamma_u}N_1N_4\left(n_x+n_y\right)d\Gamma\end{pmatrix} \quad (11)$$

where $\dot{\boldsymbol{E}}$ is the first-order derivative of the electric field in time, and v refers to the transmission velocity of electromagnetic waves of medium. Therefore, the damping matrix of the boundary $\boldsymbol{F}$ can be expressed as

$$\boldsymbol{F}=\sum_{\Omega}\boldsymbol{F}_e=\sum_{\Omega}(\int_{\Gamma_l}\frac{\partial \boldsymbol{E}^T}{\partial n}\boldsymbol{N}d\Gamma+\int_{\Gamma_d}\frac{\partial \boldsymbol{E}^T}{\partial n}\boldsymbol{N}d\Gamma+\int_{\Gamma_r}\frac{\partial \boldsymbol{E}^T}{\partial n}\boldsymbol{N}d\Gamma+\int_{\Gamma_u}\frac{\partial \boldsymbol{E}^T}{\partial n}\boldsymbol{N}d\Gamma). \quad (12)$$

By importing boundary damping matrix into the GPR finite element equation, we can obtained

$$\boldsymbol{M}\ddot{\boldsymbol{E}}+\left(\boldsymbol{K}'+\boldsymbol{F}\right)\dot{\boldsymbol{E}}+\boldsymbol{K}\boldsymbol{E}=\boldsymbol{S}_E. \quad (13)$$

3.2 Sarma absorbing boundary

The Sarma absorbing boundary is a kind of attenuating absorbing layer. The basic principle is that an absorbing layer is added the boundaries of the simulation model to absorb the incident GPR waves. The medium of the absorbing layer is a kind of high attenuation characteristic media. The attenuation coefficient of the absorbing layer should be built on reasonable physical theory, and expressed as function of media parameters. Sarma (Sarma et al., 1998) proposed an absorbing boundary condition by adding an attenuating layer of a certain thickness around the boundaries area according to the material property to estimate the constant proportion coefficient. Figure 1(a) shows a sketch of the Sarma boundary condition. Rayleigh gives a classic method to calculate the damping matrix $\boldsymbol{F}$ .This method uses the whole mass matrix $\boldsymbol{M}$ and total stiffness matrix $\boldsymbol{K}$ to calculate damping matrix $\boldsymbol{F}$ .The matrix $\boldsymbol{F}$ can be expressed as

$$\left[\boldsymbol{F}\right]=a_0\left[\boldsymbol{M}\right]+a_1\left[\boldsymbol{K}\right], \quad (14)$$

where a_0, a_1 can be expressed as

$$a_0=\frac{2\omega_i\omega_j\left(\xi_i\omega_j-\xi_j\omega_i\right)}{\omega_j^2-\omega_i^2},\quad a_1=\frac{2\left(\xi_j\omega_j-\xi_i\omega_i\right)}{\omega_j^2-\omega_i^2}, \quad (15)$$

The quantities, ω_i and ω_j are the inherent radiosfrequency of the i and j media, and ξ_i and ξ_j are the corresponding damping ratios, respectively. We apply the Sarma absorbing boundary to process the reflected wave. We substitute the matrix $\boldsymbol{F}$ into equation (3).Then EFM equation in the absorbing boundary area can be obtained as

$$\boldsymbol{M}\ddot{\boldsymbol{E}}+\left(\boldsymbol{K}'+\boldsymbol{F}\right)\dot{\boldsymbol{E}}+\boldsymbol{K}\boldsymbol{E}=\boldsymbol{S}, \quad (16)$$

In the absorbing layers areas, the proportionality coefficient a_0 and a_1 can be calculated according to equation (15).

3.3 UPML absorbing boundary condition

According to the electromagnetic theory, Maxwell equations in a UPML medium can be expressed as

$$\nabla\times\boldsymbol{E}=-\mathrm{j}\omega\mu\bar{\boldsymbol{S}}\cdot\boldsymbol{H} \quad (17)$$

$$\nabla\times\boldsymbol{H}=\mathrm{j}\omega\varepsilon\bar{\boldsymbol{S}}\cdot\boldsymbol{E} \quad (18)$$

where $\bar{\boldsymbol{S}}$ is a parameter which expresses the characteristic of an anisotropic medium. It can be expressed as follows in two dimensions.

$$\bar{\boldsymbol{S}}=\begin{bmatrix}s_y/s_x & 0 & 0\\ 0 & s_x/s_y & 0\\ 0 & 0 & s_xs_y\end{bmatrix} \quad (19)$$

where $s_i=1+\sigma_i/(\mathrm{j}\omega\varepsilon_0),\ \ i=x,y$

To solve rotation on both sides of Eq. (17), and put Eq. (18) into it, we can obtain

$$\frac{1}{\mu}\bar{\boldsymbol{S}}^{-1}\nabla\times\nabla\times\boldsymbol{E}=\omega^2\varepsilon\bar{\boldsymbol{S}}\cdot\boldsymbol{E} \quad (20)$$

Substitute Eq. (19) into Eq. (20) and we obtain

$$\frac{1}{\mu}\begin{bmatrix}(1+\sigma_x/(\mathrm{j}\omega\varepsilon))^2 & 0 & 0\\ 0 & (1+\sigma_y/(\mathrm{j}\omega\varepsilon))^2 & 0\\ 0 & 0 & 1\end{bmatrix}\nabla\times\nabla\times\boldsymbol{E}= \omega^2\varepsilon\cdot\begin{bmatrix}(1+\sigma_y/(\mathrm{j}\omega\varepsilon))^2 & 0 & 0\\ 0 & (1+\sigma_x/(\mathrm{j}\omega\varepsilon))^2 & 0\\ 0 & 0 & (1+\sigma_x/(\mathrm{j}\omega\varepsilon))^2(1+\sigma_y/(\mathrm{j}\omega\varepsilon))^2\end{bmatrix}\cdot\boldsymbol{E} \tag{21}$$

Apply Fourier transform to the above equation, and we can obtain

$$\frac{1}{\mu}\nabla\times\nabla\times\boldsymbol{E}+\frac{2}{\mu\varepsilon_0}\boldsymbol{I}\frac{\partial\nabla\times\nabla\times\boldsymbol{E}}{\partial t}+\frac{1}{\mu\varepsilon_0^2}\boldsymbol{I}^2\frac{\partial\nabla\times\nabla\times\boldsymbol{E}}{\partial t^2}$$
$$=-\varepsilon\cdot\frac{\partial\boldsymbol{E}}{\partial t^2}-\frac{2\varepsilon}{\varepsilon_0}(\boldsymbol{J}+\boldsymbol{K})\cdot\frac{\partial\boldsymbol{E}}{\partial t}-\frac{\varepsilon}{\varepsilon_0^2}(\boldsymbol{J}^2+\boldsymbol{K}^2+2\cdot\boldsymbol{H})\cdot\boldsymbol{E}-\frac{2\varepsilon}{\varepsilon_0^3}\boldsymbol{K}\cdot\boldsymbol{H}\int_0^t\boldsymbol{E}\mathrm{d}t-\frac{\varepsilon}{\varepsilon_0^4}\boldsymbol{H}\cdot\int_0^t\int_0^t\boldsymbol{E}\mathrm{d}t\mathrm{d}t \tag{22}$$

Applying theGalerkin method [15] to Eq. (22), the FEM equation in a UPML medium can be expressed as

$$\boldsymbol{M}\ddot{\boldsymbol{E}}+\boldsymbol{M}_1\dot{\boldsymbol{E}}+\boldsymbol{M}_2\boldsymbol{E}+\boldsymbol{M}_3\int_0^t\boldsymbol{E}\mathrm{d}t+\boldsymbol{M}_4\int_0^t\int_0^t\boldsymbol{E}\mathrm{d}t\mathrm{d}t-\boldsymbol{K}\boldsymbol{E}-\boldsymbol{K}_1\dot{\boldsymbol{E}}-\boldsymbol{K}_2\ddot{\boldsymbol{E}}=\boldsymbol{S} \tag{23}$$

The express of the matrixes in Eq. (23) is as follows

$$\begin{cases}\boldsymbol{M}=\int_e\boldsymbol{N}^{\mathrm{T}}\boldsymbol{N}\mathrm{d}\Omega\\ \boldsymbol{K}=\frac{1}{\mu\varepsilon}\int_e\left(\frac{\partial\boldsymbol{N}}{\partial x}\left(\frac{\partial\boldsymbol{N}}{\partial x}\right)^{\mathrm{T}}+\frac{\partial\boldsymbol{N}}{\partial y}\left(\frac{\partial\boldsymbol{N}}{\partial y}\right)^{\mathrm{T}}\right)\mathrm{d}\Omega\end{cases}\quad\begin{cases}\boldsymbol{M}_1=\frac{2}{\varepsilon_0}(\boldsymbol{J}+\boldsymbol{K})\int_e\boldsymbol{N}^{\mathrm{T}}\boldsymbol{N}\mathrm{d}\Omega\\ \boldsymbol{K}_1=\frac{2}{\mu\varepsilon_0\varepsilon}\boldsymbol{I}\int_e\left(\frac{\partial\boldsymbol{N}}{\partial x}\left(\frac{\partial\boldsymbol{N}}{\partial x}\right)^{\mathrm{T}}+\frac{\partial\boldsymbol{N}}{\partial y}\left(\frac{\partial\boldsymbol{N}}{\partial y}\right)^{\mathrm{T}}\right)\mathrm{d}\Omega\end{cases}$$

$$\begin{cases}\boldsymbol{M}_2=\frac{1}{\varepsilon_0^{\,2}}(\boldsymbol{J}^2+\boldsymbol{K}^2+2\cdot\boldsymbol{H})\int_e\boldsymbol{N}^{\mathrm{T}}\boldsymbol{N}\mathrm{d}\Omega\\ \boldsymbol{K}_2=\frac{1}{\mu\varepsilon_0^{\,2}\varepsilon}\boldsymbol{I}^2\int_e\left(\frac{\partial\boldsymbol{N}}{\partial x}\left(\frac{\partial\boldsymbol{N}}{\partial x}\right)^{\mathrm{T}}+\frac{\partial\boldsymbol{N}}{\partial y}\left(\frac{\partial\boldsymbol{N}}{\partial y}\right)^{\mathrm{T}}\right)\mathrm{d}\Omega\end{cases}\quad\begin{cases}\boldsymbol{M}_3=\frac{2}{\varepsilon_0^{\,3}}\boldsymbol{K}\cdot\boldsymbol{H}\int_e\boldsymbol{N}^{\mathrm{T}}\boldsymbol{N}\mathrm{d}\Omega\\ \boldsymbol{M}_4=\frac{1}{\varepsilon_0^{\,4}}\boldsymbol{H}\int_e\boldsymbol{N}^{\mathrm{T}}\boldsymbol{N}\mathrm{d}\Omega\end{cases}$$

$$\boldsymbol{I}=\begin{bmatrix}\sigma_x & 0 & 0\\ 0 & \sigma_y & 0\\ 0 & 0 & 0\end{bmatrix},\ \boldsymbol{J}=\begin{bmatrix}\sigma_y & 0 & 0\\ 0 & \sigma_x & 0\\ 0 & 0 & 0\end{bmatrix},\ \boldsymbol{K}=\begin{bmatrix}0 & 0 & 0\\ 0 & 0 & 0\\ 0 & 0 & \sigma_x+\sigma_y\end{bmatrix},\ \boldsymbol{H}=\begin{bmatrix}0 & 0 & 0\\ 0 & 0 & 0\\ 0 & 0 & \sigma_x\cdot\sigma_y\end{bmatrix}.$$

IV. Comparison test and results

To illustrate absorption effectson the incident waves at the artificially truncated boundary using different absorbing boundary condition, a 10 m × 10 m homogeneous model was established, with a pulse excitation source located at the center of the simulation area, as shown in Fig. 1. The wavelte of the GPR pulse excitation source is $f(t)=t^2e^{-\alpha t}\sin\omega_0 t$, where ω_0 is the central frequency of the transmitting antenna (in this example, ω_0=100 MHz). The attenuation velocity is governed by the coefficient α, which in this case equals to $0.93\omega_0$. The sampling interval time is 0.1 ns. The dielectric constant of the medium is $\varepsilon=6.5$, the conductivity $\sigma=0.002$ S/m, and the mesh element size = 0.0025 m^2. Absorption effects resulting from different absorbing boundary conditions were observed by wave-field snapshots at various times. Fig.2. Fig. 3 and Fig. 4 show the snapshots of wave-field surrounded by transmitting boundary condition, Sarma boundary condition and UPML boundary condition respectively. In Fig. 2, we can see that the GPR wave reaches the edge of the area at 32 ns, and the reflected wave begins to form at the artificial truncated boundary. In the snapshot at 38 ns, we can see the GPR wave energy reflected strongly by the artificial truncated boundary, greatly affecting the target area. This also indicates the necessity for effective processing of artificial truncated boundaries. Fig. 3 and Fig. 4 show wave field snapshots at 12, 32 and 38 ns by using the transmitting boundary condition and Sarmaboundary condition respectively. As seen in the figures, wave energy again reaches the boundary area at 32 ns. By 38 ns, however, the majority of the electromagnetic wave energy has been transmitted through the boundary, with only a small portion reflected back. By comparison to the energy of the strongly reflected wave on the truncated

boundary at the same time (Fig. 5(c)), we see that the transmitting boundary condition and Sarmaboundary condition has a remarkable effect. However, wave field snapshot of 32 ns shows that there is still some reflected energy from the truncated boundary. Compared with Fig. 3 and Fig. 4, wave filed snapshots of 32 ns in Fig. 5 which is by using UPML absorbing boundary condition have perfectly absorbing effect, the reflected wave are nearly absorbing.

Fig. 6.showsthe recorded signal and their envelope at point A in Fig. 1 under different absorbing boundary conditions. The recorded signal contains the transmission signal and the reflected signal from the boundary. From these figures we can see that under the UPML boundary condition, the reflected energy is least. The refection efficient of no absorbing boundary condition， transmitting boundary condition, sarmaboundary condition and UPML boundary condition calculated after a spreading correction ofthe wave front are -9.68 dB, -24.8 dB, -34.7 dB,-55.8 dB respectively. Compared with other two absorbing boundary conditions, the UPML boundary condition has best absorbing effect.

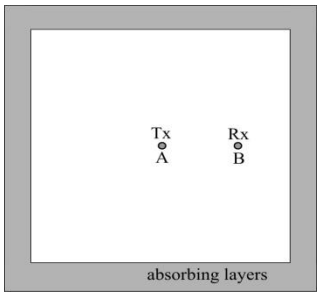

Fig.1. Sketch drawing of the Sarma boundary condition model

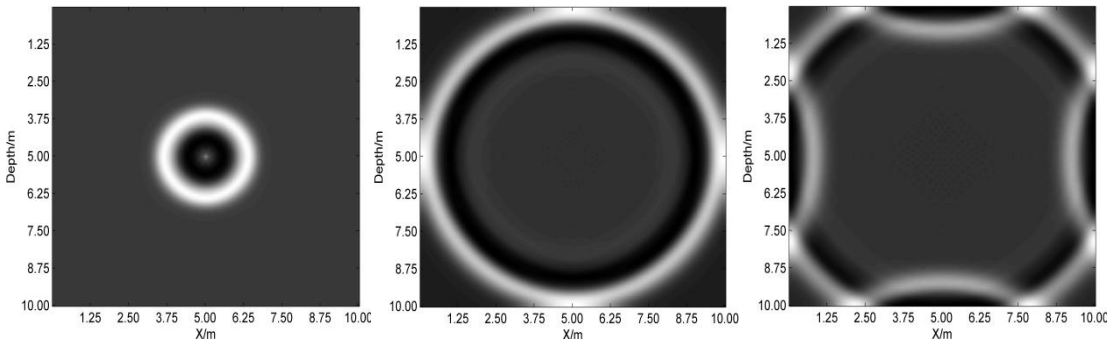

(a) 12 ns snapshot(b) 32 ns snapshot (c)38 ns snapshot

Fig.2.Snapshots of wave field without boundary conditions

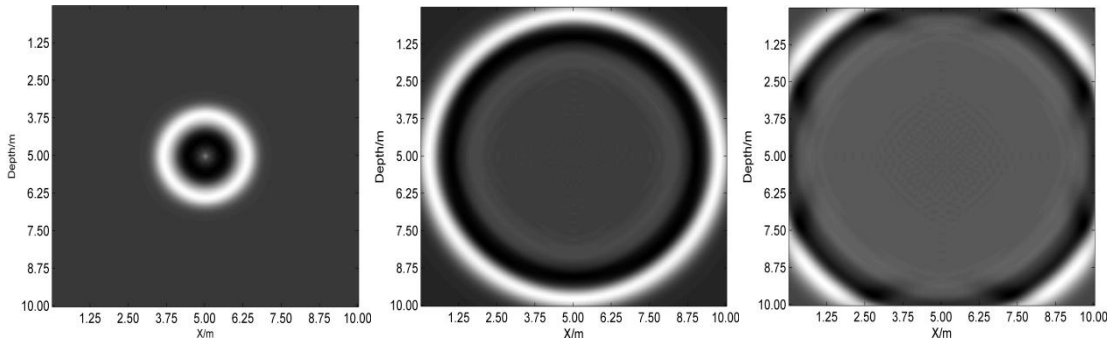

(a)12 ns snapshot (b) 32 ns snapshot(c) 38 ns snapshot

Fig.3. Snapshots of wave field with the transmitting boundary condi

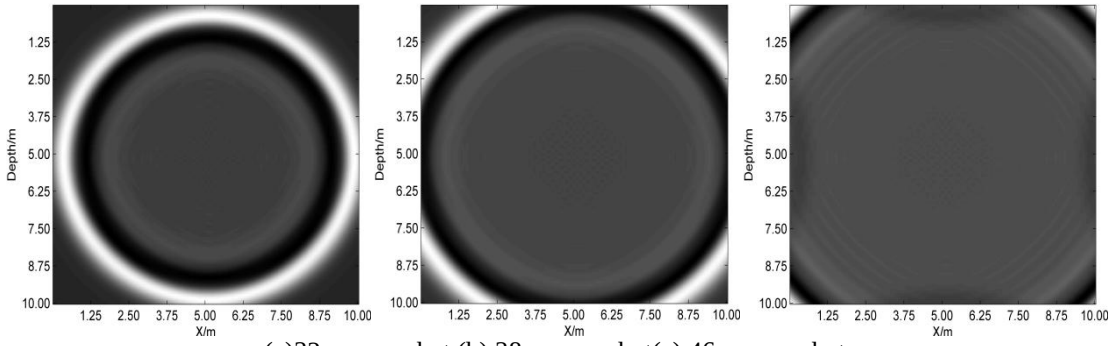

(a)32 ns snapshot (b) 38 ns snapshot(c) 46 ns snapshot

Fig.4. Snapshots of wave field with Sarma absorbing boundary condition

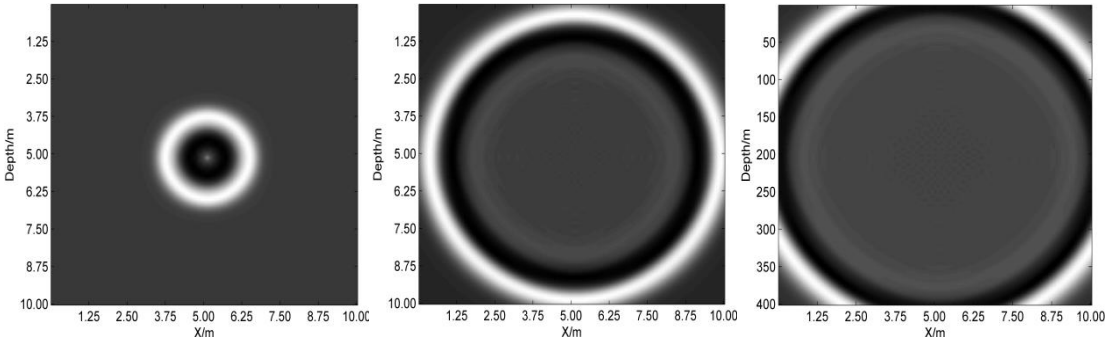

(a)12 ns snapshot (b) 32 ns snapshot(c) 38 ns snapshot

Fig.5. Snapshots of wave field ts with the UPML boundary condition

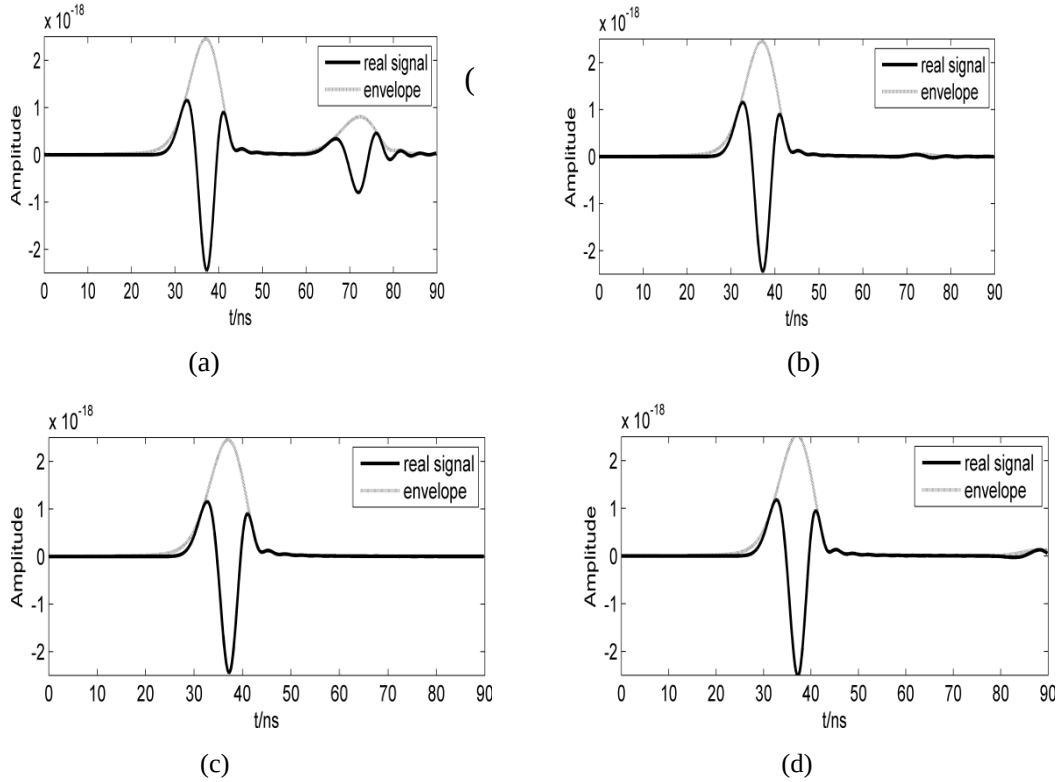

(a) (b)

(c) (d)

Fig.6. Incident and reflected signal from different absorbing boundary. (a) No absorbing boundary condition;(b) Transmitting boundary condition; (c) Sarma absorbing boundary condition and (d) UPML absorbing boundary condition.

IV. Conclusion

Transmitting boundary condition, Sarma absorbing boundary condition and UPML absorbing boundary condition for simulation of ground penetrating radar (GPR) by the time domain finite element (FEM) method are described and compared by the reflection coefficient.The results demonstrated that UPML boundary condition can yield a reflection coefficient smaller than -50 dB, which -20 dB smaller than other two boundary conditions.

Acknowledgments

This work has been supported by the National Natural Science Foundation of China (Nos. 41304056 and41304055).

REFERENCES

[1.] B.Shen,Study of radar wave equation and its forward modeling. Geophysical and Geochemical computation technology, 16(1,)1994,29-33.(in Chinese)

[2.] Q.Y. Di, and M.Y.Wang, 2D finite element modeling for radar wave. Chinese Journal of Geophysics, 42(6), 1999, 818-825. (in Chinese)

[3.] L. Tiao, W. Cai, and P.W. Zhang, Discontinuous Galerkin Time-Domain Method forGPR Simulation in Dispersive Media. IEEE Transactions on Geoscience and Remote Sensing, 43(1), 2005, 72-80.

[4.] P. Arias, J. Armesto, and D. Capua, Digital photogrammetry, GPR and computational analysis of structural damages in a mediaeval bridge. Engineering Failure Analysis, 14(8), 2007,1444-1457.

[5.] A Bayliss,and E.Turkel, Boundary conditions for the helmholtz equation in duct-like geometries. IntAssoc for Mathematics & Computers in Simulation, 1982, 455-458.

[6.] B Engquist, and A.MajdaAbsorbing boundary conditions for numerical simulation of waves. Proc.Conf. on the National Academy of Sciences, America, 1977, 1765-1766.

[7.] K. K. Mei,and Jiayuan.Fang,Superabsorption - A method to improve absorbing boundary conditions. IEEE Transactions on Antennas and Propagation, 40(9, 1992, 1001-1010.

[8.] S. D. Gedney, G.Liu, and J. A.Roden, Perfectly Matched Layer Media With CFS For An Unconditionally Stable ADI-FDTD Method.IEEE Transactions on Antennas and Propagation, 49 (11), 2001, 1554-1559.

[9.] J P.Berenger, A perfectly matched layer for the absorption of electromagnetic waves.Journal ofComputational Physics, 114 (2), 1994, 185-200.

[10.] G.Mur, Absorbing boundary conditions for the finite-difference approximation of the time-domain electromagnetic-field equations, IEEE Transactions on Electromagnetic Compatibility, 23(4), 1981, 377-382.

[11.] Q Y. Di, M G. Zhang, and M Y. Wang, Migration of groundpenetrating radar data with a finiteelement method that considers attenuation and dispersion, geophysics, 69(2), 2005, 472-477.

[12.] D S. Feng, C S. Chen, and H H. Wang, Finite element method GPR forward simulation based on mixed boundary condition. Chinese journal of geophysics, 55(11), 2012, 3773-3785.

[13.] S Z. Xu, Finite element method for geophysics.(Science Press,1994).

[14.] C. Cerjan, D. Kosloff, and M. Reshef, A nonreflecting boundary condition for discrete acoustic and elastic wave equation. Geophysics, 50, 1985, 705-708.

[15.] D C. Xu, S X. Wang, and S J.Jiao, Wave equation finite-element modeling including rugged topography and complicated medium. Progress in Geophysics, 22(2), 2007, 522-529.

[16.] J F.Claerbout, Imaging the Earth's Interior, (Blackwell Scientific Publications, 1985).

[17.] G S. Sarma, K. Mallick, and V R. Gadhinglajkar, Nonreflectingboundary condition in finite element formulation for an elastic wave equation. Geophysics, 63(3),1998, 1006-1016

[18.] J F. Semblat, A. Gandomzadeh, and L. Lenti, A simple numerical absorbing layer method in elastodynamics, ComptesRendusMecanique, 338, 2010, 24-32

[19.] D S. Feng,and Q w. Dai, GPR numerical simulation of full wave field based on UPML boundarycondition of ADI-FDTD. NDT&E International,44(6), 2011, 495-504.

[20.] J. Li, Z F. Zeng,L. Huang, and F S.Liu, GPRsimulation based on complex frequency shifted recursiveintegration PML boundary of 3D high order FDTD, Computers and Geosciences, 49,2012, 121-130.